Waveguiding at the Edge of a Three-Dimensional Photonic Crystal

Ling Lu (陆凌), John D. Joannopoulos, and Marin Soljačić

Waveguiding at the edge of a three-dimensional photonic crystal

Ling Lu (陆凌), John Joannopoulos and Marin Soljačić

Department of Physics, Massachusetts Institute of Technology, Cambridge, Massachusetts 02139, USA

We find that electromagnetic waves can be guided at the edge of a three-dimensional photonic crystal in air. When the waveguide is defined by the intersection of two surface planes, the edge modes are associated with the corresponding surface bands. A simple cell counting approach is presented to describe the periodic evolution of the system with interesting interplays among edge, surface and bulk states.

An electron can be bounded in the bulk (3D), surface (2D), edge (1D)[1] or corner (0D) of a three-dimensional (3D) electronic crystal in vacuum. But a photon doesn't see vacuum as a potential barrier as an electron does. At the vacuum or air interface, a photonic mode can be bounded (having infinite lifetime) if all its wavevectors are larger in amplitude than its vacuum wavevector (the total-internal-reflection requirement). This condition cannot be satisfied for zero-dimensional (0D) cavity-type modes whose mode extension is finite in all spatial directions. Exposed to air, 1D waveguide-type modes are thus the bound states of the lowest dimension in photonics. In the context of photonic crystals (PhCs)[2] in air, interfacial bound states have been found to exist at the edges of 2D PhCs[3] and at the surfaces[4, 5] of 3D PhCs. These two types of bound states are both reductions by one dimension from their bulk states. Similarly, a plasmonic wedge mode[6, 7] (that is intrinsically lossy) is also a reduction by one dimension from its 2D states, since there are no bulk electromagnetic modes in metals where the dielectric constant is negative. In contrast, we present here the 1D edge mode of 3D PhCs; it is a reduction by two dimensions from 3D bulk through 2D surfaces: this phenomenon has thus far not been explored. Tuning the surface terminations of a 3D PhC edge-structure can uniquely lead to photonic states whose dimensionality evolves through all three dimensions: to and from bulk, surface and edge modes. In addition, recent developments of nano-fabrication[8–11] are bringing 3D PhC devices closer to realization. In any finite-sized device applications, the existence of not only the known 2D surface states but also the 1D edge states should be taken into account during the design. Last but not the least, the potential connection between the topologically protected edge states and the gapped surface or bulk [12–15] is another interesting aspect that motivates us for this study. In this letter, we present a systematic study of the 1D edge modes of a 3D PhC in air; these results can potentially stimulate additional design rules for 3D PhC devices, novel waveguiding schemes and new "topological insulators" in photonics.

In order to confine an electromagnetic mode at a PhC edge in air, it should have a decay solution in bulk, surface and air. This requires a simultaneous bulk and surface gap underneath the light-line. First, we adopt the diamond lattice shown in Fig. 1(a), which has the largest bandgap known so far[16, 17]. Furthermore, most of the popular 3D PhC structures are diamond-like[18] and the properties of their surface states[2, 4] have been studied. Second, we pick $\langle 110 \rangle$[23] as
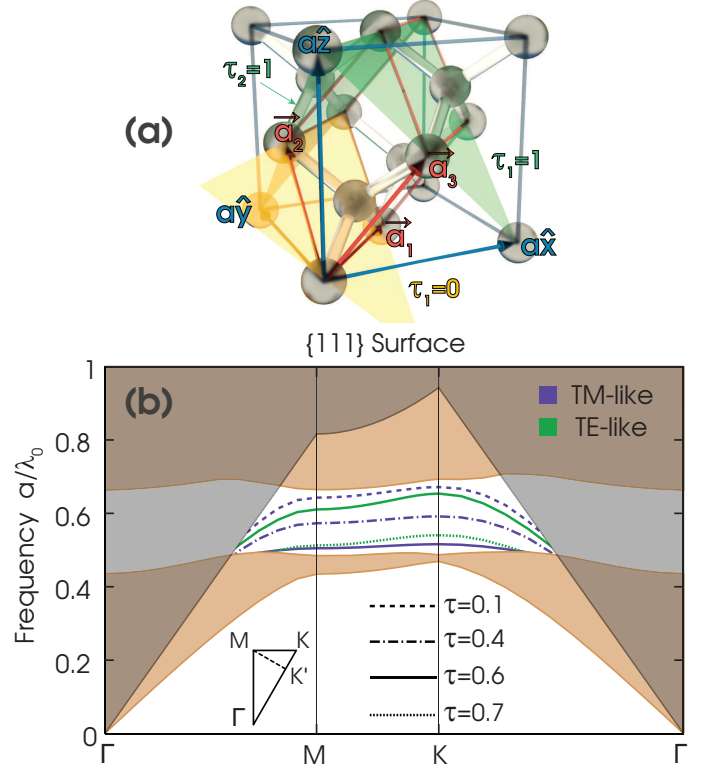

FIG. 1: (a) Illustration of a diamond lattice. The cubic unit cell of length a is outlined in blue and the fcc primitive cell is outlined in red. Two $(1\bar{1}1)$ surfaces of equivalent termination parameters $\tau_1 = 0$ and $\tau_1 = 1$ are shown in yellow and green. They lie on the end faces of the fcc primitive cell connected by $\vec{a}_3$. The $(\bar{1}11)$ surface of $\tau_2 = 1$ is also shown in green. Any of the two intersecting planes define the [110] edge along $\vec{a}_1$. $\hat{v}$ ($\equiv \frac{\vec{v}}{|\vec{v}|}$) represents a unit vector along $\vec{v}$. (b) The projected bandstructure of the $\{111\}$ surfaces of the inverse diamond PhC in air. The $\{111\}$ surfaces, containing a C_{3v} symmetry, have a triangular lattice of lattice constant $a/\sqrt{2}$. The brown area is the projected bulk modes. The light-cone is shaded in transparent gray. The irreducible BZ is shown as an inset. Γ-K' is the irreducible BZ of the edge waveguide along the $\langle 110 \rangle$ directions.

the directions for waveguiding. It has the shortest periodicity ($a/\sqrt{2}$) and thus provides the longest Brillouin zone(BZ) length underneath the light-line. $\langle 110 \rangle$ waveguides can be defined by any two surfaces intersecting along those directions. We choose two of the $\{111\}$ surfaces for the ease of the calculation. The calculations in this paper are performed with a supercell method using the MIT Photonic-Bands (MPB) pack-

age [19].

We first study the {111} surface modes following Ref. [4]. A termination parameter τ ($0 \le \tau < 1$) is defined to describe the plane of termination on the surface. Shown in Fig. 1(a), the face-centered-cubic (fcc) primitive cell (red lines) are enclosed by six {111} surfaces. Let one end surface be the $\tau = 0$ plane and the opposite end be the equivalent $\tau = 1$ plane. Note this convention is not the same as that in Ref. [4]. Fig. 1(b) shows the band diagram of the {111} surfaces of the inverse diamond structure with background dielectric constant of 13 and air sphere radius of $0.325a$ on every diamond lattice point. This structure has a bulk gap size of 29.6%. The confined surface dispersions under the lightline and inside the bandgap are plotted for different terminations within one cycle of the termination parameters. When τ increases from 0 to 1, exactly two[24] surface dispersions fall from the air band, across the bandgap, to the dielectric band. By dielectric and air bands[2] we mean the bulk bands under and above the bulk gap; they correspond to valence and conduction bands in electronic band theory. One of the surface dispersions contains the TE-like states whose dominant electric field component is in the surface plane; the other contains the TM-like states whose dominant magnetic field component is in plane. The surface dispersions are cut off by either the light-line or the bulk dielectric projected bands.
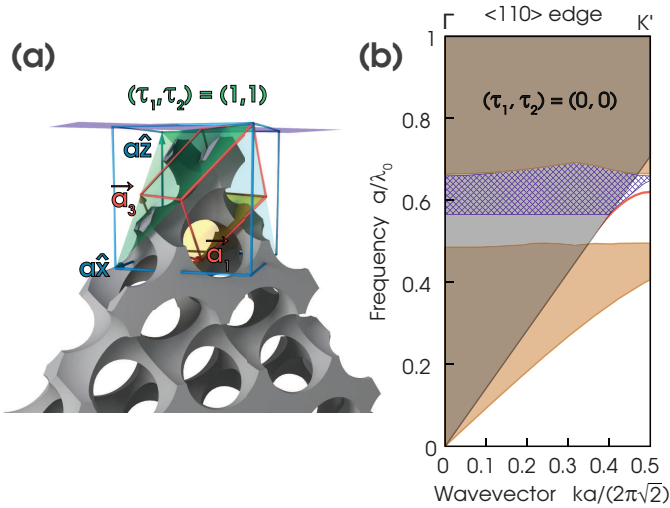

FIG. 2: (a) One unit cell of the edge waveguide along $\vec{a}_1$. The 3D PhC consists of air-spheres of diamond lattice in a dielectric matrix rendered in gray solid. The cells and {111} surfaces are the same as those in Fig. 1(a). The top purple area in the cubic cell (001) plane is the region where the 2D cuts are made in Fig. 4 and in the Supplemental Material[22]. (b) Bandstructure of the edge waveguide formed by two ⟨110⟩ surfaces, both of zero termination parameters.

The [110]($\hat{a}_1$) edge can be defined by introducing another {111} surface. In this paper, we study the edge of an acute angle (70.53°) defined by surface $(1\bar{1}1)$ and $(\bar{1}11)$ denoted by surface-1 and surface-2 respectively. The edge is determined by their termination parameters τ_1 and τ_2. From now on, we use the notation (τ_1, τ_2) to describe a specific edge geometry.

Fig. 2(a) shows the dielectric structure of the (1,1) edge. (1,1) edge is physically the same as the (0,0), (0,1) and (1,0) edges, when the bulk and surfaces are infinitely extended in space. The band diagram of this edge waveguide is shown in Fig. 2(b). The dispersion of the edge mode is drawn in red. The surface band projections of the two identical surfaces are plotted in purple and filled with slanted lines to the left and right representing the two surfaces on the left and right. The portion of the surface bands in the gray shaded region (above the light-line) are the guided surface modes projected from other directions. Since the surface dispersions are mostly isotropic in the surface BZ, the cut-offs of the surface bands in the waveguide diagram are close to a straight line above the light-line.

All the possible edges in this setup can be exhausted by tuning τ_1 and τ_2 independently from 0 to 1. We illustrate this process in Fig. 3(a) and compile the dispersion results in Fig. 3(b). In Figs. 2(b) and 3(b), all the edge dispersion curves are tied to certain surface bands. This is in contrast to the relation between surface dispersions and bulk bands in Fig. 1(b), where the surface dispersions are sweeping through the bulk gap independently of the bulk bands. The difference can be understood by considering the real space configurations in those two cases. While the surface cell can be terminated on top of the bulk cells, the edge cell (formed by cutting surfaces) is always moving along with the surface planes. This edge-surface association happens in both real and k spaces. The field distribution of an edge mode is mainly localized on the side of the surface it connects to in the band diagram. This is supported by the top two mode profiles in Fig. 4. The field of the mode in (0.4,0.0) is mainly concentrated towards surface-1; the dispersion of this mode is connected to the surface-1 band in the band diagram. The (0.0,0.4) mode is a mirror image of the (0.4,0.0) mode; it is associated with surface-2. When the two surfaces are identical, the edge modes are shared by both surfaces.

The periodic evolution of the edge unit cell can be understood through the simple heuristic in Fig. 3(a). All the primitive cells are labeled by b(bulk), s(surface) and e(edge) according to their locations. The (0,0) edge unit cell has N by N bulk cells, N surface-1 cells, N surface-2 cells and one edge cell. From (0,0) to (1,0), N surface-1 cells evolve into bulk cells; the edge cell evolves into a surface-2 cell; N+1 new cells are created to replace them. In the reciprocal space, a total number of 2(N+1) modes[24], per k point, drop in frequency to find their new homes. At the same time, the same number of modes drop from the air band to replace them. The end point (1,0) has the same spectrum as that of (0,0) except there are 2N more bulk states in the bulk dielectric band and one more state in each surface-2 bands. Calculation results of this transition are shown in band diagrams at the top row of Fig. 3(b). Due to the one to one transition between the old and new edge cells, two edge states appear during this transition. The two edge modes are associated with each surface-1 bands of different polarizations. Similar transition happens from (1,0) to (1,1).

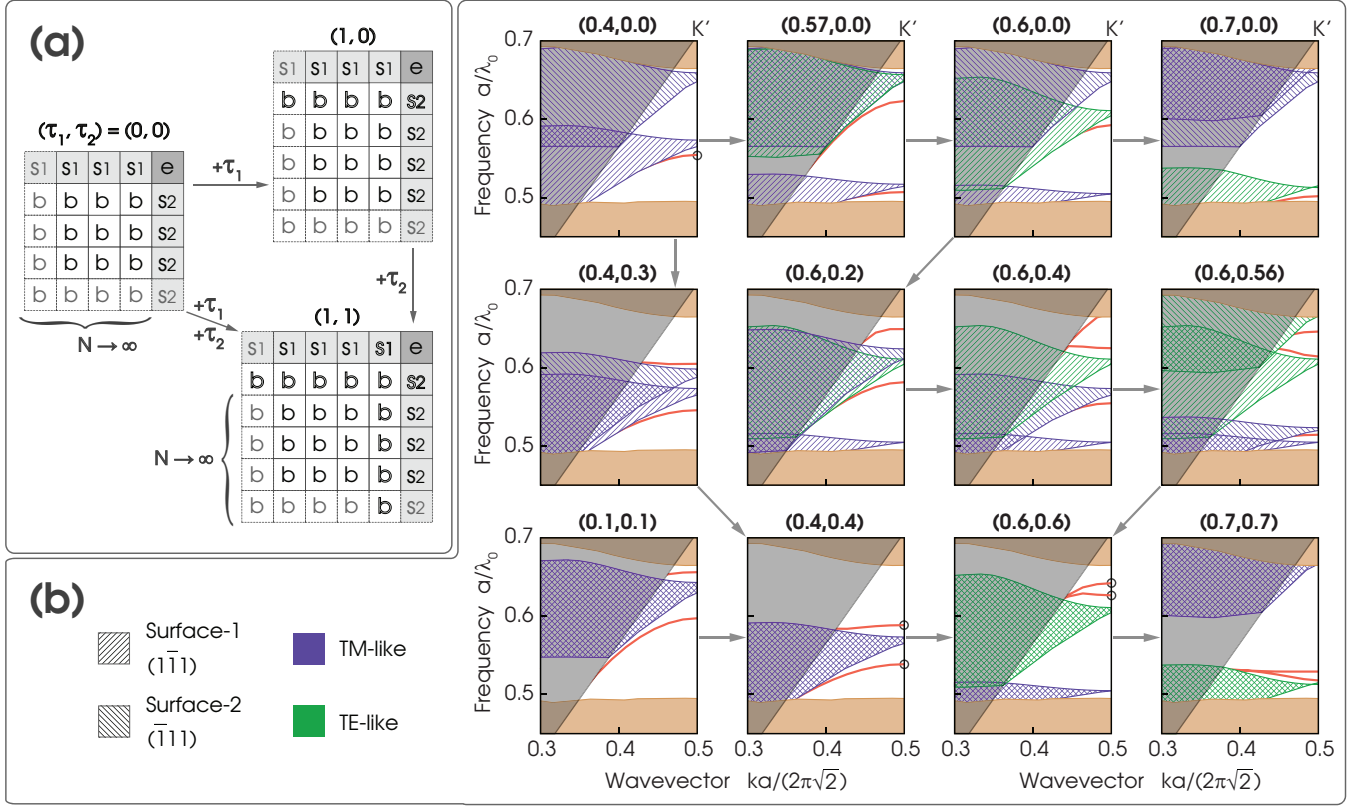When both surfaces are evolving at the same time ($\tau_1 =$

FIG. 3: (a) Schematic illustration of the periodic evolution of the edge unit cell. The cells of the outlined font indicate the increment from the original structure. By dashing the left and bottom boundaries of the structures, we mean the spatial extension of the cells beyond what is drawn. (b) Evolution of the edge dispersion diagrams of different surface terminations. The mode profiles of the circled edge dispersions at the zone boundary (K') are presented in Fig. 4 and in the Supplemental Material[22].

τ_2), the number of edge modes are doubled. The four edge modes are a result of the involvement of both the neighboring surface-1 and surface-2 cells during the edge formation. Recall for the transition from (0,0) to (1,0) or (0,1), only one surface cell is involved in edge formation. The existence of four edge modes are shown at the bottom row of the band diagrams in Fig. 3(b). In the (0.1,0.1) and (0.4,0.4) plots, there are two edge modes on each side of the TM-like surface bands. In the (0.6,0.6) and (0.7,0.7) plots, there are another two edge modes on top of the TE-like surface bands. The different frequency orderings of the two edge modes with respect to their associated surface bands are consistent with the concentration factors of the modes defined as $\frac{\int_{\varepsilon \neq 1} d^3 \mathbf{r} \varepsilon(\mathbf{r}) |\mathbf{E}(\mathbf{r})|^2}{\int d^3 \mathbf{r} \varepsilon(\mathbf{r}) |\mathbf{E}(\mathbf{r})|^2}$. The mode frequency is lower if its electric field is more concentrated in the dielectric.

The middle row of the band diagrams in Fig. 3(b) connects two of the plots in the top and bottom rows by increasing τ_2. These plots illustrate the interaction between the surface and edge bands. When τ_1 is fixed at 0.4, the increase of τ_2 from 0.0 to 0.4 pulls the TM-like surface-2 band towards the TM-like surface-1 band. One of the surface dispersions is pushed out of the surface-2 band and becomes an edge dispersion. When τ_1 is fixed at 0.6, increasing τ_2 from 0.0 to 0.6 pulls both surface-2 bands down. From (0.6,0.0) to (0.6,0.4),

the TM-like surface-2 band "exchanged" its edge mode with the TM-like surface-1 band. When an edge mode changes its surface connection, its field localization also moves from one surface to the other. From (0.6,0.4) to (0.6,0.6), the two edge modes associated with the two TE-like surface bands move through the TE-like surface-2 band and end up at the top in the (0.6,0.6) diagram.

3D vectorial field profiles of several edge modes, associated with the TM-like surface bands, are shown in Fig. 4. The symmetry of the dielectric structure is helpful in classifying the modes. In the waveguide unit cell shown in Fig. 2(a), the (110) mirror plane at $\vec{a}_1$, but perpendicular to $\vec{a}_1$, is the only point group operation that keeps the dielectric structure invariant under all termination parameters. In the waveguide BZ, Γ and K' points are invariant under this mirror operation. So the mode profiles at K' can be classified by even and odd with respect to this central mirror plane. We call the four modes in Fig. 4 odd due to the zero field intensity at the symmetry plane. When $\tau_1 = \tau_2$, we have a second mirror plane of $(1\bar{1}0)$ containing $\vec{a}_1$ and $\hat{z}$ axes. The four edge modes in the last row of Fig. 3(b) can be classified as symmetric or anti-symmetric with respect to the plane. It is evident that the lower frequency mode in (0.4,0.4) are symmetric and the other is anti-symmetric. Another interesting observation illustrated
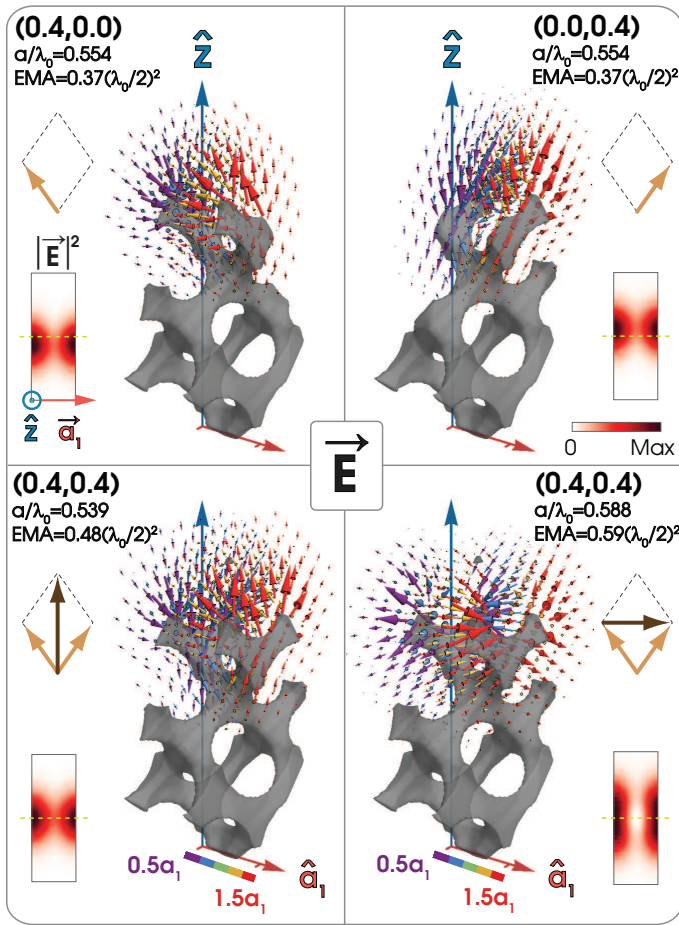
FIG. 4: Mode profiles of the edge modes associated with the TM-like surface bands at the BZ boundary(K'). The dielectric structures are drawn as transparent contour surfaces in gray. The arrows point to the directions of the electric fields; their sizes represent the field amplitudes. The colors of the arrows represent the field locations along the waveguide propagation direction($\vec{a}_1$). The fields of the amplitudes one order of magnitude less than the maximum field amplitude are not plotted. The insets on the sides of the vector plots are the plane cuts of the intensity square of the electric fields. The area and location of the plane (in air) is illustrated in Fig. 2(a). Central lines are drawn in yellow dash to indicate the mode positions.
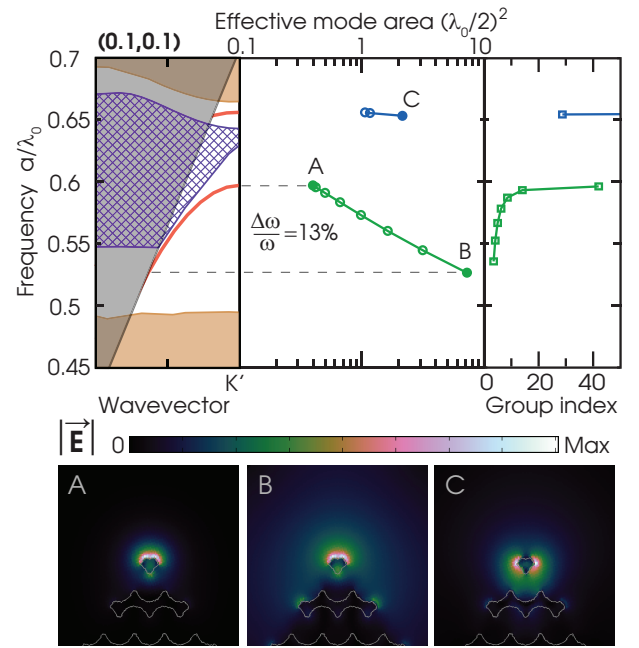

FIG. 5: Effective mode areas and group indices of the edge modes of the (0.1,0.1) edge are evaluated over their operational bandwidths. Field profiles are plotted for three representative modes with the gray outlines of the dielectric-air interfaces.

in Fig. 4 is the manifestation of the mode interaction in the their fields. The mode profiles in Fig. 4 show the field vectors of the two (0.4,0.4) modes are the addition and subtraction of the field vectors of the modes in (0.4,0.0) and (0.0,0.4). The mode profiles of the two even edge modes associated with the TE-like surface bands in (0.6,0.6) are presented in the Supplemental Material[22].

In order to evaluate the potential of the edge modes as waveguides, we present the effective mode areas (EMA), group indices and guiding bandwidths in Fig. 5 for the two edge dispersions of the (0.1,0.1) edge. The EMAs are calculated using $\frac{(\int_{vol} d^3\mathbf{r}|\mathbf{E}(\mathbf{r})|^2)^2}{\frac{a}{\sqrt{2}} \int_{vol} d^3\mathbf{r}|\mathbf{E}(\mathbf{r})|^4}$ [20]. The integration volume (vol) is the unit-cell of the waveguide which is $a/\sqrt{2}$ long in the

waveguiding direction. All these waveguide parameters are comparable to the 2D PhC air-clad membrane waveguides that have been well studied[21]. The magnitudes of the electric fields are plotted for three modes at the front surface ((110) plane at $\vec{a}_1$) of the waveguide unit-cell.

Finally, we would like to point out that the interplay between the edge, surface and bulk states can be more complicated in different edge formations. For example, the edge can be formed by two different lattice planes; the edge unit-cell can contain more than one primitive cell along the waveguiding direction; the edge can be further modified by adding or removing materials. We believe the approach and general arguments made in this paper can be adopted to study those systems and to guide the design of devices made in 3D PhCs. In those devices, engineering of the edge mode dispersions is necessary to avoid finite size effects; one can also take advantage of them to guide light into, out of, or around the bulk. The fact that an edge can be formed by two different surfaces with very sharp angles may be interesting for sensing and probing purposes. Needless to say, topologically protected edge modes of 3D PhCs are also anticipated.

[1] K. Kobayashi, Phys. Rev. B **69**, 115338 (2004).

[2] J. D. Joannopoulos, S. G. Johnson, J. N. Winn, and R. D. Meade, *Photonic Crystals: Molding the Flow of Light (Second Edition)* (Princeton University Press, 2008).

[3] W. M. Robertson, G. Arjavalingam, R. D. Meade, K. D. Brommer, A. M. Rappe, and J. D. Joannopoulos, Opt. Lett. **18**, 528 (1993).

[4] R. D. Meade, K. D. Brommer, A. M. Rappe, and J. D. Joannopoulos, Phys. Rev. B **44**, 10961 (1991).

[5] K. Ishizaki and S. Noda, Nature **460**, 367 (2009).

[6] L. Dobrzynski and A. A. Maradudin, Phys. Rev. B **6**, 3810 (1972).

[7] E. Moreno, S. G. Rodrigo, S. I. Bozhevolnyi, L. Martín-Moreno, and F. J. García-Vidal, Phys. Rev. Lett. **100**, 023901 (2008).

[8] M. Qi, E. Lidorikis, P. T. Rakich, S. G. Johnson, J. D. Joannopoulos, E. P. Ippen, and H. I. Smith, Nature **429**, 538 (2004).

[9] S. Takahashi, K. Suzuki, M. Okano, M. Imada, T. Nakamori, Y. Ota, K. Ishizaki, and S. Noda, Nat Mater **8** (2009).

[10] E. C. Nelson, N. L. Dias, K. P. Bassett, S. N. Dunham, V. Verma, M. Miyake, P. Wiltzius, J. A. Rogers, J. J. Coleman, X. Li, et al., Nat Mater **10**, 676 (2011).

[11] S. Ghadarghadr, C. P. Fucetola, L. L. Cheong, E. E. Moon, and H. I. Smith, J. Vac. Sci. Technol. B **29**, 06F401 (2011).

[12] F. D. M. Haldane and S. Raghu, Phys. Rev. Lett. **100**, 013904 (2008).

[13] Z. Wang, Y. Chong, J. D. Joannopoulos, and M. Soljacic, Nature **461**, 772 (2009).

[14] L. Fu, Phys. Rev. Lett. **106**, 106802 (2011).

[15] R.-L. Chu, J. Shi, and S.-Q. Shen, Phys. Rev. B **84**, 085312 (2011).

[16] K. M. Ho, C. T. Chan, and C. M. Soukoulis, Phys. Rev. Lett. **65**, 3152 (1990).

[17] C. T. Chan, K. M. Ho, and C. M. Soukoulis, Europhys. Lett. **16**, 563 (1991).

[18] M. Maldovan and E. L. Thomas, Nat Mater **3**, 593 (2004).

[19] S. G. Johnson and J. D. Joannopoulos, Opt. Express **8**, 173 (2001).

[20] C. Monat, B. Corcoran, D. Pudo, M. Ebnali-Heidari, C. Grillet, M. Pelusi, D. Moss, B. Eggleton, T. White, L. O'Faolain, et al., Selected Topics in Quantum Electronics, IEEE Journal of **16**, 344 (2010).

[21] T. Baba, Nat Photon **2**, 465 (2008).

[22] See supplemental material at [URL will be inserted by AIP] for the mode profiles of the two edge modes of the (0.6,0.6) edge.

[23] We use [] to identify a specific direction, $\langle \rangle$ to identify a family of equivalent directions, () to identify a specific plane and {} to identify a family of equivalent planes.

[24] In general the number of surface bands is related to the numbers of bulk bands below the gap in the BZ of the perfect crystal. There are two bands below the gap in the diamond bulk fcc primitive cell.